Volume 54 | Number 47 | 14 June 2018 | Pages 5921–6076

ChemComm

Chemical Communications

rsc.li/chemcomm

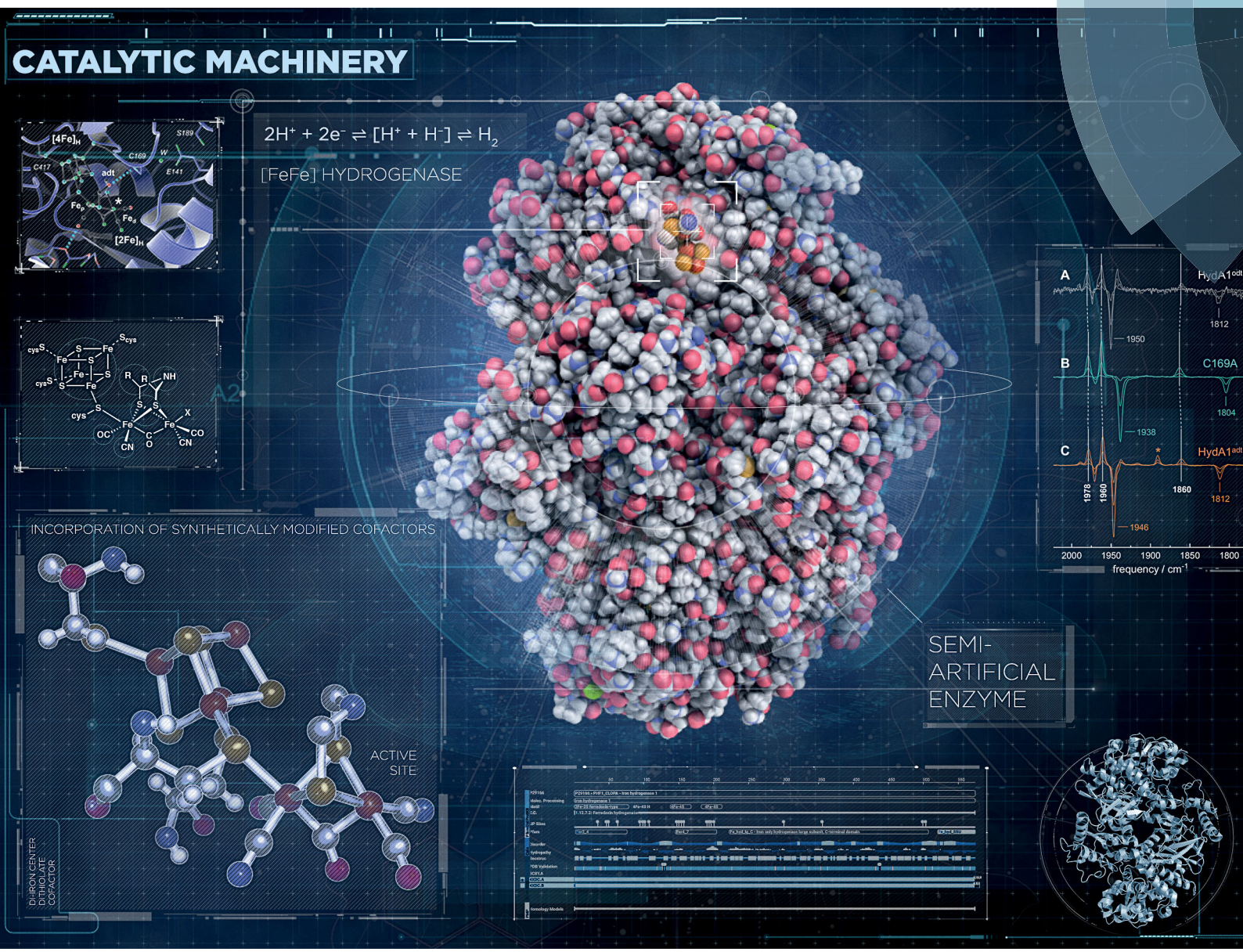

ISSN 1359-7345

ROYAL SOCIETY OF CHEMISTRY

FEATURE ARTICLE

U.-P. Apfel *et al.*

[FeFe]-Hydrogenases: recent developments and future perspectives

ChemComm

FEATURE ARTICLE

View Article Online
View Journal | View Issue

Cite this: *Chem. Commun.*, 2018, **54**, 5934

[FeFe]-Hydrogenases: recent developments and future perspectives

F. Wittkamp,[a] M. Senger,[b] S. T. Stripp [b] and U.-P. Apfel *[ac]

Received 13th February 2018,
Accepted 23rd April 2018

DOI: 10.1039/c8cc01275j

rsc.li/chemcomm

[FeFe]-Hydrogenases are the most efficient enzymes for catalytic hydrogen turnover. Their H_2 production efficiency is hitherto unrivalled. However, functional details of the catalytic machinery and possible modes of application are discussed controversially. The incorporation of synthetically modified cofactors and utilization of semi-artificial enzymes only recently allowed us to shed light on key steps of the catalytic cycle. Herein, we summarize the essential findings regarding the redox chemistry of [FeFe]-hydrogenases and discuss their catalytic hydrogen turnover. We furthermore will give an outlook on potential research activities and exploit the utilization of synthetic cofactor mimics.

Introduction

Hydrogenase enzymes are outstanding natural catalysts for the heterolytic conversion of protons and electrons into molecular hydrogen (eqn (1)).[1] Depending on the metal composition of the active site, these enzymes are divided into [NiFe]-, [FeFe]-, and [Fe]-hydrogenases. They are an important factor for adjusting the redox balance in green algae, bacteria, and archaea in H_2-based respiration processes.[2]

$$2H^+ + 2e^- \rightleftharpoons [H^+ + H^-] \rightleftharpoons H_2 \quad (1)$$

Among all hydrogenases, [FeFe]-hydrogenases show an unsurpassed H_2 release activity of up to 8.000 μmol H_2 min^{-1} mg^{-1} protein.[3] This efficiency is based on the unique design of the active site cofactor (Fig. 1A). An in-depth understanding of the hydrogenases' active site structural properties and reactivity is crucial to develop new catalysts for an efficient H_2 production.[4] The potential for technical applications of such bioinspired approaches was recently demonstrated at the example of $Fe_{4.5}Ni_{4.5}S_8$.[5–7] This mineral compound reveals striking similarities with the [NiFe]-hydrogenase cofactor (Fig. 1B) and binds bridging hydrides in the electrocatalytic generation of H_2.[8] To fully exploit the potential of biomimetic catalysis, a deeper knowledge about the molecular proceedings of enzymatic hydrogen turnover is vital including potential proton pathways, redox and spin states and cofactor geometry. In the last few years, developments in synthetic, electrochemical and spectroscopic methods have led to an improved understanding of the interplay of electrons and protons at the active site of [FeFe]-hydrogenases. In particular, site-selective protonation critically influences the electron density across the cofactor and conducts redox events in the catalytic cycle. We herein will focus on the current understanding of proton-coupled electron transport dynamics of [FeFe]-hydrogenases and recent developments in modifying the active site cofactor.

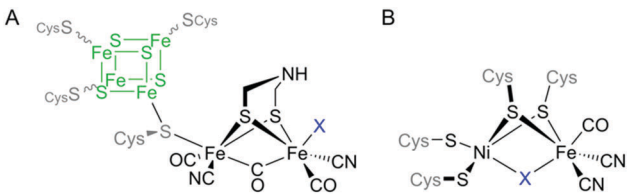

Fig. 1 Schematic representation of the active site cofactor of [FeFe]-hydrogenases (A) and [NiFe]-hydrogenases (B). The site of catalytic H_2/proton turnover is marked with X.

The cofactor of the active site

The cofactor of the [FeFe]-hydrogenases is an assembly of two distinct iron–sulphur sites, in combination referred to as the "H-cluster" (Fig. 1A and 2). Here, a cuboidal [4Fe–4S] cluster is attached to the protein scaffold by three cysteine residues ($[4Fe]_H$). This $[4Fe]_H$ cluster is connected *via* a fourth cysteine residue to a unique diiron moiety ($[2Fe]_H$) that represents the second iron–sulphur site and completes the H-cluster.[9,10] The $[4Fe]_H$ and $[2Fe]_H$ clusters are about 4 Å apart which facilitates an efficient electronic coupling. The $[2Fe]_H$ cluster is the site of catalytic turnover and thus requires a more detailed description. It consists of two iron centers in proximal (Fe_p) or distal (Fe_d) position relative to the $[4Fe]_H$ cluster. The proximal iron center is coordinated by one terminal cyanide ($_pCN^-$) and a carbonyl ligand ($_pCO$). Furthermore, it is connected to the

[a] *Faculty of Chemistry and Biochemistry, Ruhr-Universität Bochum, Universitätstrasse 150, 44801 Bochum, Germany. E-mail: ulf.apfel@rub.de*
[b] *Department of Physics, Freie Universität Berlin, Arnimallee 14, 1495 Berlin, Germany*
[c] *Fraunhofer UMSICHT, Osterfelder Strasse 3, D-46047 Oberhausen, Germany*

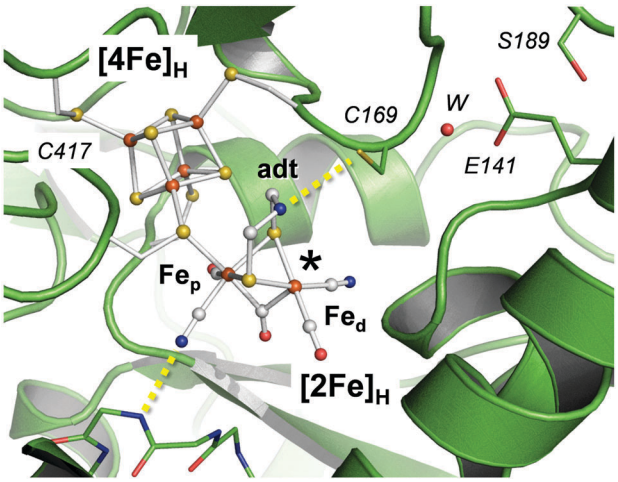

Fig. 2 Crystal structure of the [FeFe]-hydrogenase from *C. pasteurianum* (CpI, pdb coordinates 4XDC). The catalytic cofactor comprises a $[4Fe]_H$ cluster and a $[2Fe]_H$ cluster ("H-cluster"). The asterisk denotes a vacant binding site at the distal iron ion (Fe_d) of the H-cluster. Key residues are numbered with respect to HydA1, the [FeFe]-hydrogenase of *C. reinhardtii*. Potential hydrogen bonds with the protein fold have been highlighted.

$[4Fe]_H$ cluster *via* a cysteine, which is the only covalent anchor to the protein. A hydrogen bond of $_pCN^-$ to the protein scaffold further stabilizes the $[2Fe]_H$ cluster (Fig. 2).[11] The distal iron is equally coordinated by $_dCN^-$ and $_dCO$ but additionally features an open coordination site in apical position. Besides structural stabilization, the CN^- ligands are important to adjust the redox potential of the H-cluster by raising the electron density on the iron ions.[12,13] A third CO ligand bridges both iron centers (μCO) and forces Fe_d to adopt the so-called "rotated state".[14] This geometry stabilizes the open coordination site at Fe_d which is responsible for the high activity of the enzyme.

A key feature of all [FeFe]-hydrogenases is the azanediyldimethanethiolate group (adt) bridging Fe_p and Fe_d.[15–17] This moiety serves as a proton relay and is positioned at the end of an amino acid trajectory leading from the $[2Fe]_H$ site to the protein surface. Molecular dynamic (MD) simulations were employed to characterize this conserved proton transfer path.[18–21] It is formed by two glutamic acid side chains, at least one serine, one or two water molecules, and a cysteine in close vicinity to the adt group of the H-cluster (Fig. 2). Moreover, a hydrophobic gas channel connects the protein surface and the active site niche.[22] This channel, however, is unselective for H_2 and likewise allows CO and O_2 to approach the $[2Fe]_H$ center.[23] While CO reversibly inhibits the enzymes, O_2 irreversibly binds to the $[2Fe]_H$ cluster and eventually leads to degradation of the H-cluster.[24,25]

Artificial maturation

Although [FeFe]-hydrogenases are a thoroughly investigated enzyme family, there are eminent gaps in the understanding of certain redox species and their participation in the catalytic cycle. Such information is crucial to allow for a rational design of synthetic, non-noble metal catalysts. While gram-scale synthesis of potential catalysts is necessary to perform spectroscopic and kinetic investigations, isolation of large amounts of enzymes from their natural environment is cumbersome. Furthermore, a selective manipulation of the important inorganic cofactor is precluded *in vivo* and limits the possibilities to investigate reactions at specific parts of the H-cluster.

In nature, the [FeFe]-hydrogenases are activated by a specific maturation machinery consisting of HydEFG as well as the apoprotein, HydA.[26,27] Isolation of the homologously synthesized enzymes provides low yields and renders a detailed study of these enzymes challenging. Contrary to *in vivo* isolation methods, Kuchenreuther *et al.* presented a method to express [FeFe]-hydrogenases from *C. reinhardtii* (HydA1) and *C. pasteurianum* (CpI) in genetically modified *E. coli* cells.[28] This method established a significantly improved isolation protocol and facilitated the generation of up to 30 mg of purified and active [FeFe]-hydrogenase per liter cell culture. Likewise, the hydrogenase apoprotein (*i.e.* without the $[2Fe]_H$ cofactor) was obtained using the same method but in the absence of the maturase genes HydEFG.[29] The most striking result on [FeFe]-hydrogenase research was subsequently reported by Fontecave, Lubitz, and Happe in a joint project. They were able to show that maturase HydF is capable of binding and transferring an artificially synthesized cofactor mimic to apo-HydA1 and generates fully functional [FeFe]-hydrogenase enzymes.[16] An even more simplified protocol was reported briefly afterwards. Starting from inactive HydA1 apoprotein, the synthetically produced cofactor readily inserts into the enzymatic binding pocket and yields an active enzyme, most notably in the absence of HydF.[15,29,30]

The huge advantage of this approach is obvious – both apoprotein and cofactor can be obtained in gram scale. In addition, since a synthetic diiron site is added to the inactive enzyme and is not biosynthesized in parallel to the apoprotein, site-specific modifications of the $[2Fe]_H$ and $[4Fe]_H$ cluster are possible. Recently, this approach enabled for a selective enrichment of $[2Fe]_H$ with spectroscopically relevant isotopes such as ^{57}Fe allowing *e.g.* for Mössbauer- and nuclear vibrational resonance spectroscopic (NRVS) studies.[25,31,32] Following such isotopic labelling studies, the investigation of specific redox states became feasible (see below). Furthermore, non-natural variations of the $[2Fe]_H$ site such as an exchange of the bridgehead nitrogen atom (*e.g.* to CH_2, S, or O)[30,33] or replacement of the CO and/or CN^- ligands by typical inorganic coordination ligands (*e.g.* phosphines) became feasible as well.[34] While specific isotope editing is used to investigate [FeFe]-hydrogenases without interfering with the catalytic properties,[25,31,32,35] varying the elemental composition of the H-cluster can now be applied to alter the H_2 evolution performance and identify structural features fundamental for catalysis.

The incorporation of artificial cofactors can help to understand the enzymatic H_2 turnover and opens the possibility to design effective and durable catalysts. Here, almost all reported modifications of the H-cluster are located at the $[2Fe]_H$ moiety (Fig. 3) whereas the $[4Fe]_H$ cluster has not been addressed to the same extent. Chalcogenide exchange experiments have been reported for the [4Fe–4S] cluster of ferredoxin before[36–38] and the strong resemblance with the $[4Fe]_H$ cluster has drawn our attention towards a comparable exchange of the sulphides to

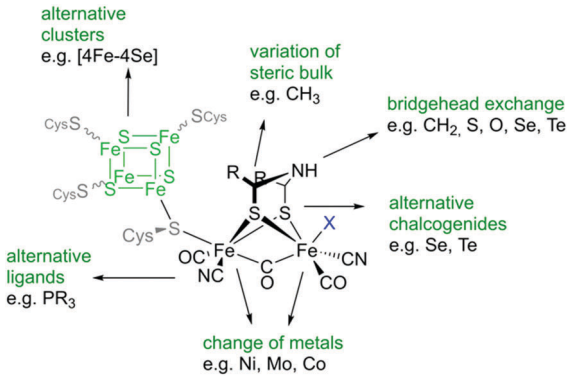

Fig. 3 Possible alterations of the H-cluster, the active site of [FeFe]-hydrogenases.[14,34,40,41]

selenides.[39] The $[4Fe]_H$ cluster can be easily incorporated into the protein *via* self-assembly from inorganic iron salts and selenides. Successful incorporation was confirmed by X-ray crystallography and anomalous scattering at the 12.666 keV edge of selenium. Such [4Fe–4Se] apoprotein was activated with the natural $[2Fe]_H$ cluster and yielded wildtype-like H_2 release activity. This behavior suggests a high tolerance of the cofactor towards electronic manipulations.

Alterations of the diiron site have stimulated tremendous attention.[30] While over 300 synthetic mimics are reported in the literature,[42] only a few were yet incorporated into the hydrogenase enzyme. Utilization of such mimics usually led to inactive enzymes since the amine of the adt group serves as intrinsic base and proton relay and is considered a crucial feature of the $[2Fe]_H$ cluster (Fig. 3). Besides the biologically relevant complex $[Fe_2(CO)_4(CN)_2\{(SCH_2)_2NH\}]^{2-}$, only $[Fe_2(CO)_5(CN)\{(SCH_2)_2NH\}]^-$ and $[Fe_2(CO)_4(CN)_2\{(SCH_2)_2NCH_3\}]^{2-}$ revealed recognizable H_2 release activity.[30] These results indicate that both CN^- ligands and the "right" basicity of the proton relay site are of utmost importance for hydrogen turnover. Therefore, it seems obvious that in order to retain enzyme-like activity a potential mimic should contain two CN^- ligands and the adt dithiolate. We subsequently took the next step and replaced the bridging thiolates of the $[2Fe]_H$ cluster by selenides.[43] In line with reports on chalcogenide replacements within synthetic mimics, we expected that this S/Se exchange will lead to enhanced catalytic activity, *e.g.* due to an increase of electron density at the diiron site and optimized electron transfer, accordingly.[41,44–46] Maturation with the synthetic adSe cluster was performed[47] and yielded the selenium-modified HydA1 and CpI variants. The modified hydrogenases revealed a slightly increased H_2 release activity as compared to the wildtype enzyme. Notably, catalytic activity was biased towards proton reduction. This imbalance between H_2 release and uptake is most likely due to the increased electron density at the diiron site as is also shown by a bathochromic "red shift" in the IR signature of the H-cluster compared to native $[2Fe]_H$.

The redox states

Although numerous enzymatic intermediates were observed and spectroscopically characterized, the details of [FeFe]-hydrogenase turnover are not fully understood. Only recently with the improved maturation protocols sufficient amounts of protein became available to perform in-depth enzyme studies on the various reported intermediates. Among these intermediates, there is only little debate concerning the oxidized species of the enzyme. H_{ox} and H_{ox}–CO as well as their protonated counterparts $H_{ox}H$ and $H_{ox}H$–CO[48] are all characterized by a $[2Fe]_H^{3+}$ site with both iron ions adopting a low-spin state and an oxidized $[4Fe–4S]^{2+}$ cluster.[49] The presumed charge asymmetry in H_{ox} (Fe_p^I–Fe_d^{II}) is less pronounced in H_{ox}–CO.[49] Since the electron distribution in the $[2Fe]_H$ cluster is still a matter of debate, we will only present the formal overall charge of the diiron site. There is consensus that H_{ox} is the resting state of the enzyme and exhibits an open coordination site for substrate binding to Fe_d (* in Fig. 2). As a result of combining real-time attenuated total reflection Fourier-transform infrared spectroscopy (ATR-FTIR) and density functional theory (DFT), we could recently assign the individual vibrational modes of H_{ox} and H_{ox}–CO using a specific isotopic editing protocol.[35] Exposure to ^{13}CO gas in combination with blue or red light irradiation facilitated the generation of eight possible H_{ox} and 16 H_{ox}–CO isotopomers.

In general, H_{ox} shows three strong stretching frequencies, assigned to the Fe–Fe bridging carbonyl (μCO, 1802 cm^{-1}), the terminal CO ligand at Fe_d ($_dCO$, 1940 cm^{-1}) as well as that at Fe_p ($_pCO$, 1964 cm^{-1}).[52] These modes are largely uncoupled and agree well with theoretical models that feature all-equatorial CO and CN^- ligands at Fe_d and Fe_p as depicted in Fig. 4A.[35] Interestingly, distortions of the octahedral geometry at Fe_d as shown in Fig. 4B are well compatible with the experimental frequencies and suggest significant rotational freedom at the site of catalysis. Upon CO gas exposure, a fourth band at higher IR frequencies appears that is indicative of an additional CO ligand at Fe_d. This is a unique feature of the catalytically inhibited H_{ox}–CO state.[52] While it was previously believed that the additional CO molecule blocks the vacant binding site of H_{ox} ("standard" geometry as in Fig. 4C),[53] recent IR spectroscopic

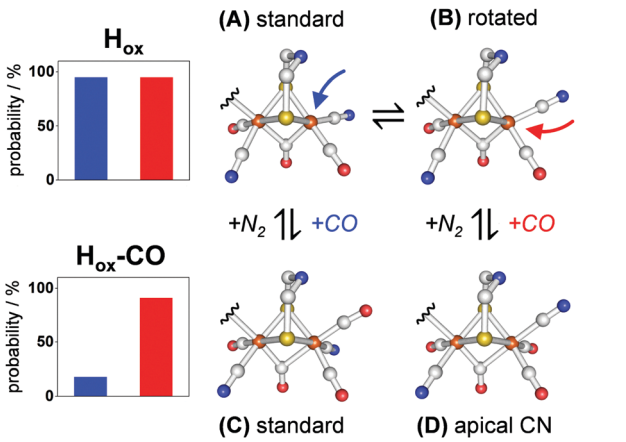

Fig. 4 H-Cluster rotamers of H_{ox} and H_{ox}–CO and their probability distribution. Both H_{ox} rotamers A and B are equally probable while upon CO inhibition, the apical CN^- rotamer (D) is clearly favoured over the "standard" geometry (C). The arrows suggest a possible trajectory for CO to attack on Fe_d. Original data from Senger *et al.*[35]

investigations and DFT calculations suggest that herein a rotamer with an apical CN^- is more likely (Fig. 4D).[35] The lack of evidence for an electrostatic interaction between Fe_d–CN^- and the protein, however, still allows for speculations on Fe_d rotamers[54] and even more substantial differences in cofactor geometry of other intermediates.[55–57]

Upon acidification of the enzyme samples, the IR spectrum of H_{ox} reveals the formation of a new species with an up-shift of 4–6 cm^{-1} for all terminal ligands and up to 10 cm^{-1} higher values for μCO.[48] The formation of this species depends on the pH value and is fully reversible upon increasing the pH to alkaline conditions. This hypsochromic "blue shift" does not occur in the absence of a reductant although the increase of frequencies suggests a lower electron density at $[2Fe]_H$. Both one-electron reduction and oxidation of the diiron site lead to significantly higher IR shifts.[58] The small shift observed for all CO/CN^- bands upon acidification thus has to correspond to a novel, protonated redox state and was accordingly labelled $H_{ox}H$.[48] Likewise, bacterial [FeFe]-hydrogenases showed this behavior suggesting the protonated $H_{ox}H$ species to be an omnipresent intermediate in [FeFe]-hydrogenases. In addition, the IR shift is not affected by changes in the protein surrounding the cofactor as shown for amino acid variants containing modifications at cysteine 169 (Fig. 2) as well as chemical cofactor variations (*e.g.* $HydA1^{pdt}$). Likewise, the blue shift cannot be assigned to a protonation of Fe_d since H_{ox}–CO revealed a similar up-shift of cofactor bands. Acidification under a CO atmosphere subsequently leads to a new intermediate that was named $H_{ox}H$–CO. Even upon S/Se chalcogenide exchange at the $[4Fe]_H$ cluster,[39] a comparable shift of the CO bands was observed that eliminates the sulphides of the cuboidal cluster as a potential protonation site.[59–61] In the C169A variant, proton transfer towards the adt-ligand is blocked. Therefore, the protonation reaction must be independent of this pathway. The X-ray structure of apo-$HydA1$[29] reveals that the $[4Fe]_H$ cluster is in direct contact with bulk water while in prokaryotic hydrogenases it is deeply buried within the protein. Here, a chain of water molecules extends from the protein surface to cysteine 417 that binds the $[4Fe]_H$ cluster (Fig. 5).[62] It was therefore assumed that this cysteine might act as a possible protonation site. This hypothesis was supported by DFT calculations and Cys417 was suggested to be the most-likely candidate for the formation of $H_{ox}H$ and $H_{ox}H$–CO.

This $[4Fe]_H$ protonation modulates the redox potential of the H-cluster.[55] After receiving a first electron, the enzyme is typically less likely to accept a second electron. Protonation of the $[4Fe]_H$ cluster may therefore compensate for the negative charge of the electron and thus the second electron can be transferred at a comparable potential. While the oxidized states generally find broad acceptance within the community, the one-electron reduced states H_{red}, $H_{red'}$, and $H_{red'}H$ as well as the inhibited state $H_{red'}$–CO and H_{sred} have been discussed controversially in recent years.[48,50,51,55,63] This mainly stems from the fact that only a limited amount of spectroscopic data was available to gain an in-depth structural understanding of the reduced intermediates. Basically all reduced intermediates were suggested before 2013, the magic year when the protocols

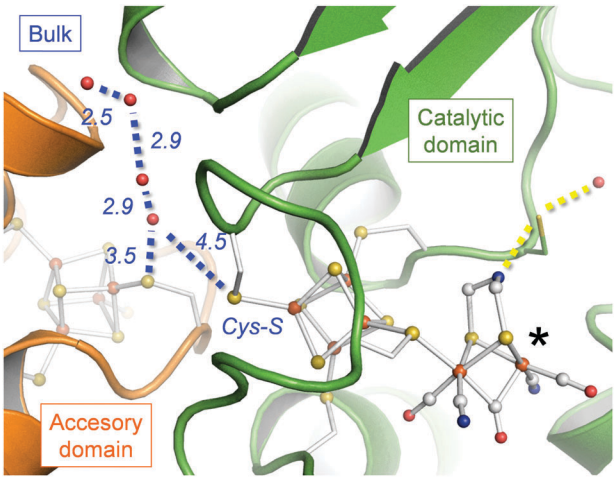

Fig. 5 Putative proton path from bulk solvent to the $[4Fe]_H$ site of the H-cluster (pdb coordinates 4XDC). In HydA1, "Cys-S" corresponds to C417. The water chain is conserved in all crystal structures and can be found in a cleft between the accessory and catalytic domain. O–O distances are given in Å (blue lines). Original data from Senger *et al.*[48]

for artificial maturation were published.[15,16] The combination of increased sample availability and the possibility to change the cofactor composition led to the observation of additional redox states. This new input raised questions about previous assumptions on the role of the different reduced states.

To allow the reader to follow the upcoming discussion, we like to refer to the nomenclature assigned in Table 1. Starting from the resting state H_{ox}, reduction of the $[2Fe]_H$ site results in a species, formerly assigned as H_{red}.[50,63] This state is characterized by CO bands at 1962 cm^{-1}, 1915 cm^{-1} and 1891 cm^{-1}. Since Mössbauer studies revealed an oxidized $[4Fe]_H^{2+}$ cluster for H_{red},[64,65] the $[2Fe]_H$ site was therefore assigned to $[2Fe]_H^{2+}$, well in line with the largely bathochromically shifted CO bands in comparison to H_{ox}. The reduced diiron site is paramagnetic (Table 1). An $[4Fe]_H^{+}$–$[2Fe]_H^{3+}$ intermediate could be observed as well ($H_{red'}$, Fig. 6A). To investigate this state in detail, the semi-artificial enzyme version $HydA1^{pdt}$ was utilized. This cofactor variant cannot adopt the H_{red} state due to the absence of the NH relay site.[48] However, the IR spectra of the accessible states H_{ox} and $H_{red'}$ reveal almost identical CO shift patterns as compared to the wildtype enzyme. At pH 8 and in a pure H_2 atmosphere, the IR pattern of H_{ox} fully disappears in favour of new CO bands at 1962 cm^{-1}, 1934 cm^{-1} and 1798 cm^{-1}. Under acidic conditions and otherwise identical experimental settings, likewise slightly blue-shifted frequencies with respect to $H_{red'}$ were observed. This behavior suggests the existence of an additional intermediate denoted as $H_{red'}H$.[48] Recent spectro-electrochemical measurements show that the formation of both one-electron reduced species is pH- and potential-dependent. Furthermore, both intermediates are linked by a proton-coupled rearrangement.[48,51] While the $[4Fe]_H^{2+}$–$[2Fe]_H^{2+}$ configuration of H_{red} dominates at acidic pH, the $[4Fe]_H^{+}$–$[2Fe]_H^{3+}$ intermediate ($H_{red'}$) can be enriched at more alkaline pH values.[48] The combination of IR experiments and DFT frequency calculations allowed for the evaluation of different

Table 1 Catalytic intermediates of [FeFe]-hydrogenase HYDA1 and vibronic properties

Redox species		H_{ox}	$H_{red'}$	H_{red}	H_{sred}	H_{hyd}	H_{ox}–CO	$H_{red'}$–CO	$H_{ox}H$	$H_{red'}H$	$H_{ox}H$–CO
$[4Fe–4S]_H$		2+	1+	2+	1+	1+	2+	1+	2+	1+	2+
Formal charge of Fe_p/Fe_d within $[2Fe]_H$		I/II	I/II	I/I	I/I	II/II	I/II	I/II	I/II	I/II	I/II
IR frequency [cm^{-1}]	CN^-	2088, 2070	2084, 2066	2070, 2033	2068, 2026	2087, 2076	2091, 2081	—	2092, 2074	2086, 2068	2094, 2086
	CO	1964, 1940, 1802	1962, 1933, 1792	1961, 1915, 1891	1953, 1918, 1882	1978, 1960, 1860	2012, 1968, 1962, 1808	2002, 1967, 1951, 1792	1970, 1946, 1812	1966, 1938, 1800	2006, 1972, 1966, 1816
Alternative annotation			H_{red}, $H_{red'}$ [50]	$H_{red}H^+$ [51]	$H_{sred}H^+$ [51]			$H_{red'}$–CO [50]			

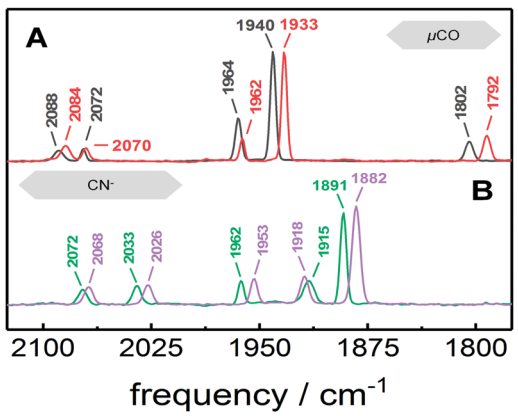

Fig. 6 Experimental IR spectra of HydA1. (A) Species with a 3+ oxidized diiron site are H_{ox} (black) and $H_{red'}$ (red). (B) Species with a 2+ reduced diiron site are H_{red} (green) and H_{sred} (magenta). Note the lack of a μCO signal and the increased gap between the CN^- bands in (B). Original data taken from Mebs *et al.*[56]

H-cluster geometries. Fig. 6 illustrates that a reduction of the diiron site from $[2Fe]_H^{3+}$ to $[2Fe]_H^{2+}$ induces a down-shift of up to ~50 cm^{-1} for single bands. In comparison, the one-electron transition $H_{ox} \rightarrow H_{red'}$ or $H_{red} \rightarrow H_{sred}$ results in a red shift for the CO bands no larger than ~10 cm^{-1}. Calculations of $H_{red'}$ favored an additional protonation of the $[4Fe]_H$ cluster, just as observed for the $H_{ox} \rightarrow H_{ox}H$ transition. Again, the best correlation between measured and calculated IR spectra was found for an additional protonation at C417 (Fig. 5, Cys-S).

These results clearly showed that the $H_{red'}$ intermediate is a one-electron reduced species comprising a reduced $[4Fe]^+$ cluster and a H_{ox}-like $[2Fe]_H$ cluster in terms of valence (I/II) and geometry (*i.e.* an open binding site and bridging CO ligand). The structural relation of $H_{red'}$ and H_{ox} is visible by the distinct IR signals as displayed in Fig. 6A.[56] The IR pattern of H_{red}, however, clearly indicates a significant structural change within the $[2Fe]_H$ moiety, *e.g.* the loss of the low-frequency band assigned to μCO. To elucidate the structure of H_{red}, DFT calculations with (i) a hydrogen species at Fe_d and with conservative μCO geometry,[54] (ii) protonation at N(adt) with a "semi-bridging" CO at Fe_d,[51] and (iii) a Fe–Fe bridging hydride (μH) were performed.[57] Best agreement of experimental and calculated spectra was observed for a $[2Fe]_H$ site comprising a bridging hydride. Additionally, only the μH geometry reproduced the specific down shift of the CN^- ligand band characteristic for H_{red}. Therefore, H_{red} was assigned to comprise a $[4Fe]_H^{2+}$–$[Fe(\mu H)Fe]^{2+}$ cluster.[56]

Two double-reduced H-cluster intermediates have been identified, H_{hyd} and H_{sred}. The latter is formed upon reduction of H_{red} and has been characterized by EPR and FTIR spectroscopy as a paramagnetic intermediate of potential catalytic relevance.[66] The low *g*-values suggest a reduced $[4Fe]_H^+$ cluster and the CO frequencies at 1953, 1919 and 1882 cm^{-1} closely resemble the IR signature of H_{red} (Fig. 6B). This observation suggests a similar cofactor geometry. As for H_{red}, best agreement between experimental and calculated frequencies was obtained for model structures comprising a bridging hydride in a $[4Fe]_H^+$–$[Fe(\mu H)Fe]^{2+}$ assembly.[56]

An intermediate of more recent prominence is the so-called hydride state, H_{hyd}. The name originates from the assumption that a terminal hydride species necessarily should play a key role in the heterolytic formation of H_2.[67] H_{hyd} was independently identified by three groups, which shows the significance of this particular intermediate. Mulder *et al.* observed the H_{hyd} state in the C169S variant of HydA1.[68,69] This modified version of the [FeFe]-hydrogenase from *C. reinhardtii* reveals a diminished H_2 release activity due to an impaired proton conductivity and facilitated an enrichment of the H_{hyd} state in the presence of H_2 (Fig. 7B). Mössbauer studies on the C169S variants suggested that H_{hyd} consists of a reduced $[4Fe]_H^+$ cluster coupled to a "superoxidized" $[2Fe]_H^{4+}$ cluster.[68] EPR spectroscopy further supported this electronic assignment by an $S = 1/2$ rhombic 2.07 signal.[68] The transition potential of −430 mV *vs.* SHE for the population of H_{hyd} at pH 8 fits the catalytic properties of [FeFe]-hydrogenases much better than H_{sred}.[66] Additionally, FTIR spectroscopy revealed a small shift of the bridging CO band upon changing the solvent and atmosphere from H_2O/H_2 to D_2O/D_2. This behavior is consistent with an H/D exchange of the ligand in *trans* position to the μCO moiety and suggests the formation of a terminal hydride (tH) in the amino acid variant C169S.[69]

A clean IR spectrum of H_{hyd} in native HydA1 enzyme was obtained by accumulation of H_{hyd} upon concerted increase of

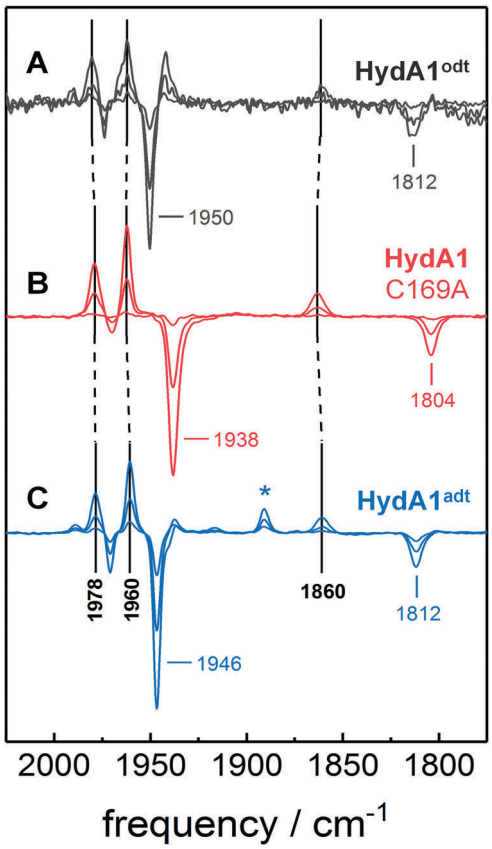

Fig. 7 Real-time ATR-FTIR accumulation of H_{hyd} over H_{ox} in presence of H_2. (A) HydA1 cofactor variant odt in black, (B) HydA1 amino acid variant C169A in red, and (C) wildtype enzyme HydA1^{adt} in blue. Negative bands are assigned to H_{ox} or $H_{ox}H$ (for wildtype enzyme), positive bands represent H_{hyd}. In HydA1^{adt} traces of H_{red} are formed (*). Original data taken from Winkler *et al.*[33]

substrate and product concentration, *i.e.* H_2 and H^+.[33] The spectra showed a dominant species with bands at 1978, 1960 and 1860 cm^{-1} (Fig. 7C) and correlate well with the observations by Mulder *et al.*[69] Furthermore, it was demonstrated that the hydride species exclusively stems from the H_2 or D_2 substrate and not the solvent. Similar results were obtained using native DdH and CpI enzymes. At neutral pH, accumulation of the H_{hyd} intermediate can be observed upon decreasing the humidity levels of the protein sample. The lack of bulk water as the acceptor molecule herein may increase the number of protons "stuck" inside the protein and was suggested to show effects comparable to acidification. This also agrees with the findings of Mulder *et al.*[68] and it seems that a disturbed proton transport pathway (PTP) is prerequisite for an accumulation of H_{hyd}. In an alternative approach as was described by Lubitz and co-workers,[31,70] a variation of the bridgehead atom of $[2Fe]_H$ led to equally suppressed proton conductivity. The semi-artificial [FeFe]-hydrogenases with an ether bridge (HydA1^{odt}; odt = oxydimethanethiolate) indeed revealed neither catalytic proton reduction nor H_2 oxidation catalysis. Fig. 7A shows the H_{hyd}/H_{ox} difference spectra for HydA1^{odt} as recorded by real-time ATR-FTIR spectroscopy.

FTIR spectroscopy is a powerful tool to analyze the active site cofactor of [FeFe]-hydrogenases and to determine changes in electron density or evaluate the geometry of otherwise transient intermediates. However, the artificial maturation pathways paved the way to apply spectroscopic methods that can give additional and direct information on the $[2Fe]_H$ cluster by selectively installing specific probes within the H-cluster. For example, a semi-artificial HydA1 enzyme comprising a Fe^{57} labelling solely at the $[2Fe]_H$ moiety was synthesized and it allowed for characterizing intermediates *via* nuclear resonance vibrational spectroscopy (NRVS).[25,31,32] Such NRVS studies on Fe^{57} enriched enzyme variants finally enabled the direct observation of a terminal hydride and confirmed the $[4Fe]_H^+$–$[2Fe(tH)]^{2+}$ assignment for H_{hyd}. In addition the first step of the oxidative degradation (O_2 deactivation) was unequivocally shown to proceed *via* an iron bound hydroperoxide ligand.[25]

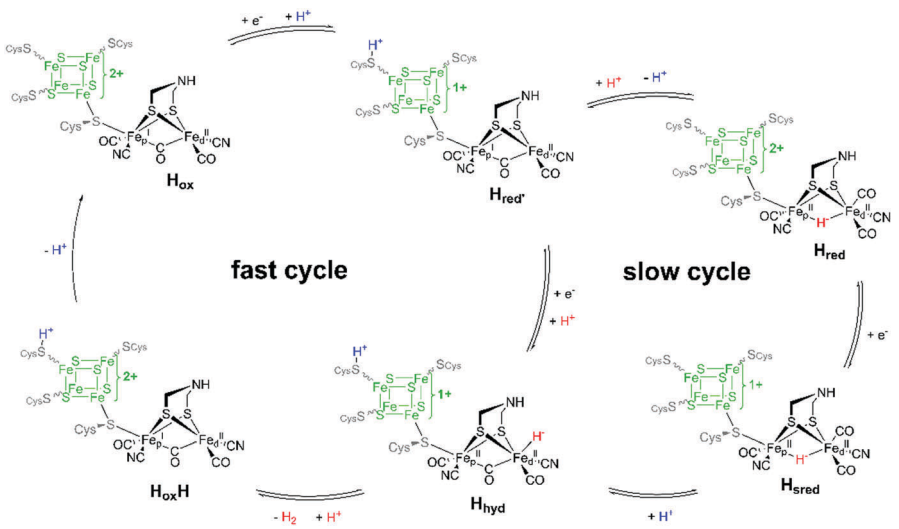

Scheme 1 Proposed catalytic cycle. Note the conservative μCO-geometry in the "fast cycle". See text for details.

The catalytic cycle

In the previous chapter, we reviewed recent attempts to identify the electronic structure of particular H-cluster intermediates. This made it indispensable to also reconsider the catalytic mechanism of the H_2 formation. An updated catalytic cycle is shown in Scheme 1. In a first step, H_{ox} is converted to $H_{red'}$ by a proton-coupled electron transfer (PCET) to the $[4Fe]_H$ cluster.[55] This PCET renders the formation of $H_{red'}$ charge neutral and may facilitate a second reduction step at a similar redox potential. The $H_{ox} \rightarrow H_{red'}$ transition appears more likely than a direct conversion into H_{red} which would result in drastic ligand reorientation and loss of the "rotated structure".[71] While $H_{red'}$ is preferably formed at alkaline pH, H_{red} accumulated under neutral or slightly acidic conditions.[48] Higher proton concentrations lead to a preferential protonation of the $[2Fe]_H$ site and withdrawal of electron density from the $[4Fe]_H$ cluster resulting in a bridging hydride. Subsequent reduction of H_{red} leads to H_{sred} that carries a bridging hydride as well.[56] The μH^- ligand is thermodynamically more stable than a terminal hydride and bridging hydride species of mimetic model complexes were shown to react only slowly with additional protons in the H_2 release reaction.[72] Therefore, the participation of H_{red} and H_{sred} as catalytic intermediates in hydrogen turnover must be questioned. This statement becomes even more evident when considering that the formation of H_{hyd} from H_{sred} requires another re-organization of geometry (Scheme 1). It has to be assumed that H_{sred} and H_{red} are a part of a slower H_2 formation pathway, *e.g.* as "signalling states" in regulatory [FeFe]-hydrogenases.[73]

Scheme 1 shows an alternative pathway. Here, protonation and reduction of $H_{red'}$ is suggested to lead to the formation of H_{hyd}. This state exhibits an apical hydride and does not require significant structural re-organization. In addition, it was shown that such hydride intermediates react rapidly with protons to form H_2, facilitating fast turnover within the enzyme.[72] Further protonation of H_{hyd} heterolytically yields H_2 and recovers the protonated resting state, $H_{ox}H$. While $H_{ox}H$ has the same structure and valence as H_{ox} it still carries an additional proton at the $[4Fe]_H$ cluster.[48] After losing this "regulatory" proton, H_{ox} is formed again and the catalytic cycle can start over again.

In summary, a fast and efficient H_2 release is only feasible upon conversion of the μCO-geometry and PCET to both the $[4Fe]_H$ cluster and Fe_d of the $[2Fe]_H$ site. The H-cluster is charged with two electrons to allow for an instant reduction of a proton into a highly reactive apical hydride. In the end, this hydride reacts in a simple acid/base reaction with an additional proton to generate hydrogen.

Conclusion and outlook

Over the past three decades, significant efforts were undertaken to understand [FeFe]-hydrogenases and mimic their catalytic activity.[1,74,75] It was, however, just recently that a major breakthrough in the understanding of the molecular proceedings of catalysis was achieved. The protocol for artificial maturation established by Fontecave, Happe and Lubitz allowed for the production of large amounts of active enzymes and site-selective modifications of the unique cofactor.[15,16] In addition, synthetic variants of the $[2Fe]_H$ and $[4Fe]_H$ cluster facilitating studies of catalytic intermediates were not available to spectroscopy before.[31,55,68] The example of [FeFe]-hydrogenases shows how in a truly interdisciplinary way chemists, biologists and physicists discovered a new path to elucidate the catalytic cycle of this interesting class of metalloenzymes.

Despite the progress within this research field, numerous points still need to be addressed. This includes the reaction of [FeFe]-hydrogenases with molecular oxygen and the subsequent decomposition of the active site. An O_2-oxididized intermediate was identified just recently,[25] supporting earlier attempts to explain the O_2 sensitivity of [FeFe]-hydrogenases by an oxygenase subroutine that converts O_2 as a substrate into reactive oxygen species (ROS).[76] Whether these ROS attack the diiron site, $[4Fe]_H$ cluster, or protein fold remains elusive.[24,77] Related to this area, the minutiae of oxidative inactivation in the absence of O_2 are barely understood. The process is of interest as the DdH enzyme has been shown to adopt the so-called H_{inact} state when isolated in the presence of air.[58] The enzyme is on stand-by, does not show hydrogen turnover in this state (hence the name), and is completely resistant to O_2. Upon reductive activation, H_{ox} is formed and the [FeFe]-hydrogenase is rendered turnover-active and O_2-sensitive. [FeFe]-Hydrogenases as analysed by protein film voltammetry (PFV) undergo inactivation at potentials exceeding +50 mV *vs.* SHE.[23] It is, however, unclear, whether this observation is related to the formation of H_{inact} or H_{trans} (an intermediate state in the H_{inact}/H_{ox} redox conversion) and what ligand might protect the enzyme from O_2 damage.

The electron exchange between the active site cofactor, accessory clusters, and external electron donors is relatively well understood.[78–81] In comparison, proton transfer to the catalytic cofactor has not been shown experimentally yet. Selective proton transfer may well be the reason for the outstanding catalytic performance of [FeFe]-hydrogenases. Potentially involved amino acids have been identified due to phylogenetic conservation[82] and MD simulations.[18–21] However, cysteine 169 of the proton relay group at the cofactor (Fig. 2) is the only residue that has been verified to propel proton transfer to and from the H-cluster.[68,69] The lack of an immediate trigger to induce a protonation reaction renders the experimental identification of involved amino acids challenging.

In addition, time-resolved IR spectroscopy on [FeFe]-hydrogenases has been demonstrated by Hammarström and Dyer.[83,84] Here, continuous wave quantum cascade lasers (QCL) are employed as probing light of high energy density. This allows measuring single frequencies with nanosecond time resolution.[85] It can be expected that steady-state FTIR spectroscopy and QCL IR spectroscopy will help in identifying catalytically relevant redox species. Furthermore, a correlation of changes in the cofactor regime with differences in the amide region will include protein structural changes in the analysis of [FeFe]-hydrogenases.

In the future, the artificial maturation of [FeFe]-hydrogenases might lead to cofactor variants with severely altered properties and reaction pathways. As a result of such enzyme manipulations, hitherto unknown enzyme reactivities might be induced.

Likewise, the altered enzyme might be utilized in the conversion of formaldehyde to methanol or even in enantioselective hydrogenation reactions with biologically non-relevant substrates, *e.g.* for the synthesis of flurbiprofen which is an important non-steroidal antiinflammatory drug.[86] Likewise, such variations might lead to more robust enzyme variants that reveal increased oxygen stability or higher H_2 release activity. Such ''improved'' behavior might, in the very end, enable the application of [FeFe]-hydrogenases in large scale bio-based H_2 generators which is currently not possible.

The small amount of synthetic biomimetic model complexes tested in the natural enzyme environment and the even smaller number of mimics affording active enzymes, however, raise the question on structural demands for suitable synthetic mimics. It will be thus of eminent interest to elucidate if any altered dithiolate moiety is capable of facilitating a wild-type like proton relay mechanism. Likewise, altered metal contents or co-ligands might allow us to establish enzymes with altered chemical properties and are thus, although laborious and demanding, an interesting target.

In conclusion, the artificial maturation enabled us and other scientists to obtain new insight into the chemistry of [FeFe]-hydrogenases within a very short time frame. Functional details of the catalytic machinery that were previously discussed controversially could now be analysed *via* hitherto unamenable spectroscopic methods. With this incorporation, likewise new information on key steps of the catalytic cycle was obtained and enzyme variants with biologically non-relevant cofactors were established.

It is thus feasible to believe that in the near future, the remaining questions will be resolved and new enzyme variants with designed properties and reactivities will be accessible.

Conflicts of interest

There are no conflicts to declare.

Acknowledgements

U.-P. A. is grateful for the financial support by the Fonds of the Chemical Industry (Liebig grant), and the Deutsche Forschungsgemeinschaft (Emmy Noether grant to U.-P. A., AP242/2-1). F. W. thanks the Studienstiftung des deutschen Volkes for a PhD fellowship. M. S. and S. T. S. acknowledge funding by the IMPRS on Multiscale Biosystems and Focus Area NanoScale.

Notes and references

1 W. Lubitz, H. Ogata, O. Rüdiger and E. Reijerse, *Chem. Rev.*, 2014, **114**, 4081–4148.
2 P. M. Vignais and B. Billoud, *Chem. Rev.*, 2007, **107**, 4206–4272.
3 S. T. Stripp and T. Happe, *Dalton Trans.*, 2009, 9960.
4 F. Möller, S. Piontek, R. G. Miller and U.-P. Apfel, *Chem. – Eur. J.*, 2018, **24**, 1471–1493.
5 S. Piontek, C. Andronescu, A. Zaichenko, B. Konkena, K. Junge Puring, B. Marler, H. Antoni, I. Sinev, M. Muhler, D. Mollenhauer, B. Roldan Cuenya, W. Schuhmann and U.-P. Apfel, *ACS Catal.*, 2018, 987–996.
6 B. Konkena, K. Junge Puring, I. Sinev, S. Piontek, O. Khavryuchenko, J. P. Dürholt, R. Schmid, H. Tüysüz, M. Muhler, W. Schuhmann and U.-P. Apfel, *Nat. Commun.*, 2016, **7**, 12269.
7 C. L. Bentley, C. Andronescu, M. Smialkowski, M. Kang, T. Tarnev, B. Marler, P. R. Unwin, U.-P. Apfel and W. Schuhmann, *Angew. Chem., Int. Ed.*, 2018, **56**, 16503.
8 I. Zegkinoglou, A. Zendegani, I. Sinev, S. Kunze, H. Mistry, H. S. Jeon, J. Zhao, M. Y. Hu, E. E. Alp, S. Piontek, M. Smialkowski, U.-P. Apfel, F. Körmann, J. Neugebauer, T. Hickel and B. Roldan Cuenya, *J. Am. Chem. Soc.*, 2017, **139**, 14360–14363.
9 J. W. Peters, W. N. Lanzilotta, B. J. Lemon and L. C. Seefeldt, *Science*, 1998, **282**, 1853–1858.
10 Y. Nicolet, C. Piras, P. Legrand, C. E. Hatchikian and J. C. Fontecilla-Camps, *Structure*, 1999, **7**, 13–23.
11 O. Lampret, A. Adamska-Venkatesh, H. Konegger, F. Wittkamp, U.-P. Apfel, E. J. Reijerse, W. Lubitz, O. Rüdiger, T. Happe and M. Winkler, *J. Am. Chem. Soc.*, 2017, **139**, 18222–18230.
12 A. Silakov, M. T. Olsen, S. Sproules, E. J. Reijerse, T. B. Rauchfuss and W. Lubitz, *Inorg. Chem.*, 2012, **51**, 8617–8628.
13 J. I. van der Vlugt, T. B. Rauchfuss and S. R. Wilson, *Chem. – Eur. J.*, 2006, **12**, 90–98.
14 M. L. Singleton, N. Bhuvanesh, J. H. Reibenspies and M. Y. Darensbourg, *Angew. Chem., Int. Ed.*, 2008, **47**, 9492–9495.
15 J. Esselborn, C. Lambertz, A. Adamska-Venkatesh, T. Simmons, G. Berggren, J. Noth, J. Siebel, A. Hemschemeier, V. Artero, E. Reijerse, M. Fontecave, W. Lubitz and T. Happe, *Nat. Chem. Biol.*, 2013, **9**, 607–609.
16 G. Berggren, A. Adamska, C. Lambertz, T. R. Simmons, J. Esselborn, M. Atta, S. Gambarelli, J.-M. Mouesca, E. Reijerse, W. Lubitz, T. Happe, V. Artero and M. Fontecave, *Nature*, 2013, **499**, 66–69.
17 A. Silakov, B. Wenk, E. Reijerse and W. Lubitz, *Phys. Chem. Chem. Phys.*, 2009, **11**, 6592.
18 G. Hong, A. J. Cornish, E. L. Hegg and R. Pachter, *Biochim. Biophys. Acta, Bioenerg., 2011*, 1807, 510–517.
19 A. J. Cornish, B. Ginovska, A. Thelen, J. C. S. da Silva, T. A. Soares, S. Raugei, M. Dupuis, W. J. Shaw and E. L. Hegg, *Biochemistry*, 2016, **55**, 3165–3173.
20 B. Ginovska-Pangovska, M.-H. Ho, J. C. Linehan, Y. Cheng, M. Dupuis, S. Raugei and W. J. Shaw, *Biochim. Biophys. Acta, Bioenerg., 2014*, 1837, 131–138.
21 M. McCullagh and G. A. Voth, *J. Phys. Chem. B*, 2013, **117**, 4062–4071.
22 J. C. Fontecilla-Camps, P. Amara, C. Cavazza, Y. Nicolet and A. Volbeda, *Nature*, 2009, **460**, 814–822.
23 G. Goldet, C. Brandmayr, S. T. Stripp, T. Happe, C. Cavazza, J. C. Fontecilla-Camps and F. A. Armstrong, *J. Am. Chem. Soc.*, 2009, **131**, 14979–14989.
24 S. T. Stripp, *PNAS*, 2009, **106**, 17331–17336.
25 S. Mebs, R. Kositzki, J. Duan, M. Senger, F. Wittkamp, U.-P. Apfel, T. Happe, S. T. Stripp, M. Winkler and M. Haumann, *Biochim. Biophys. Acta, Bioenerg., 2018*, 1859, 28–41.
26 Y. Nicolet and J. C. Fontecilla-Camps, *J. Biol. Chem.*, 2012, **287**, 13532–13540.
27 D. W. Mulder, E. M. Shepard, J. E. Meuser, N. Joshi, P. W. King, M. C. Posewitz, J. B. Broderick and J. W. Peters, *Structure*, 2011, **19**, 1038–1052.
28 J. M. Kuchenreuther, C. S. Grady-Smith, A. S. Bingham, S. J. George, S. P. Cramer and J. R. Swartz, *PLoS One*, 2010, **5**, e15491.
29 J. Esselborn, N. Muraki, K. Klein, V. Engelbrecht, N. Metzler-Nolte, U.-P. Apfel, E. Hofmann, G. Kurisu and T. Happe, *Chem. Sci.*, 2016, **7**, 959–968.
30 J. F. Siebel, A. Adamska-Venkatesh, K. Weber, S. Rumpel, E. Reijerse and W. Lubitz, *Biochemistry*, 2015, **54**, 1474–1483.
31 E. J. Reijerse, C. C. Pham, V. Pelmenschikov, R. Gilbert-Wilson, A. Adamska-Venkatesh, J. F. Siebel, L. B. Gee, Y. Yoda, K. Tamasaku, W. Lubitz, T. B. Rauchfuss and S. P. Cramer, *J. Am. Chem. Soc.*, 2017, **139**, 4306–4309.
32 R. Gilbert-Wilson, J. F. Siebel, A. Adamska-Venkatesh, C. C. Pham, E. Reijerse, H. Wang, S. P. Cramer, W. Lubitz and T. B. Rauchfuss, *J. Am. Chem. Soc.*, 2015, **137**, 8998–9005.
33 M. Winkler, M. Senger, J. Duan, J. Esselborn, F. Wittkamp, E. Hofmann, U.-P. Apfel, S. T. Stripp and T. Happe, *Nat. Commun.*, 2017, **8**, 16115.
34 U.-P. Apfel, F. Y. Pétillon, P. Schollhammer, J. Talarmin and W. Weigand, in *Bioinspired Catalysis*, ed. W. Weigand and

P. Schollhammer, Wiley-VCH Verlag GmbH & Co. KGaA, Weinheim, Germany, 2014, pp. 79–104.
35 M. Senger, S. Mebs, J. Duan, F. Wittkamp, U.-P. Apfel, J. Heberle, M. Haumann and S. T. Stripp, *Proc. Natl. Acad. Sci. U. S. A.*, 2016, 201606178.
36 W. H. Orme-Johnson, R. E. Hansen, H. Beinert, J. C. Tsibris, R. C. Bartholomaus and I. C. Gunsalus, *Proc. Natl. Acad. Sci. U. S. A.*, 1968, **60**, 368–372.
37 J. Meyer, J.-M. Moulis, J. Gaillard and M. Lutz, *Advances in Inorganic Chemistry*, Elsevier, 1992, vol. 38, pp. 73–115.
38 P. C. Hallenbeck, G. N. George, R. C. Prince and R. N. F. Thorneley, *JBIC, J. Biol. Inorg. Chem.*, 2009, **14**, 673–682.
39 J. Noth, J. Esselborn, J. Güldenhaupt, A. Brünje, A. Sawyer, U.-P. Apfel, K. Gerwert, E. Hofmann, M. Winkler and T. Happe, *Angew. Chem., Int. Ed.*, 2016, **55**, 8396–8400.
40 L. R. Almazahreh, W. Imhof, J. Talarmin, P. Schollhammer, H. Görls, M. El-khateeb and W. Weigand, *Dalton Trans.*, 2015, **44**, 7177–7189.
41 M. K. Harb, U.-P. Apfel, T. Sakamoto, M. El-khateeb and W. Weigand, *Eur. J. Inorg. Chem.*, 2011, 986–993.
42 C. Tard and C. J. Pickett, *Chem. Rev.*, 2009, **109**, 2245–2274.
43 L. Kertess, F. Wittkamp, C. Sommer, J. Esselborn, O. Rüdiger, E. J. Reijerse, E. Hofmann, W. Lubitz, M. Winkler, T. Happe and U.-P. Apfel, *Dalton Trans.*, 2017, **46**, 16947–16958.
44 U.-P. Apfel, H. Görls, G. A. Felton, D. H. Evans, R. S. Glass, D. L. Lichtenberger and W. Weigand, *Helv. Chim. Acta*, 2012, **95**, 2168–2175.
45 M. K. Harb, T. Niksch, J. Windhager, H. Görls, R. Holze, L. T. Lockett, N. Okumura, D. H. Evans, R. S. Glass, D. L. Lichtenberger, M. El-khateeb and W. Weigand, *Organometallics*, 2009, **28**, 1039–1048.
46 M. K. Harb, J. Windhager, T. Niksch, H. Görls, T. Sakamoto, E. R. Smith, R. S. Glass, D. L. Lichtenberger, D. H. Evans, M. El-khateeb and W. Weigand, *Tetrahedron*, 2012, **68**, 10592–10599.
47 W. Gao, L.-C. Song, B.-S. Yin, H.-N. Zan, D.-F. Wang and H.-B. Song, *Organometallics*, 2011, **30**, 4097–4107.
48 M. Senger, S. Mebs, J. Duan, O. Shulenina, K. Laun, L. Kertess, F. Wittkamp, U.-P. Apfel, T. Happe, M. Winkler, M. Haumann and S. T. Stripp, *Phys. Chem. Chem. Phys.*, 2018, **20**, 3128–3140.
49 A. Silakov, E. J. Reijerse, S. P. J. Albracht, E. C. Hatchikian and W. Lubitz, *J. Am. Chem. Soc.*, 2007, **129**, 11447–11458.
50 A. Adamska-Venkatesh, D. Krawietz, J. Siebel, K. Weber, T. Happe, E. Reijerse and W. Lubitz, *J. Am. Chem. Soc.*, 2014, **136**, 11339–11346.
51 C. Sommer, A. Adamska-Venkatesh, K. Pawlak, J. A. Birrell, O. Rüdiger, E. J. Reijerse and W. Lubitz, *J. Am. Chem. Soc.*, 2017, **139**, 1440–1443.
52 A. L. De Lacey, C. Stadler, C. Cavazza, E. C. Hatchikian and V. M. Fernandez, *J. Am. Chem. Soc.*, 2000, **122**, 11232–11233.
53 B. J. Lemon and J. W. Peters, *Biochemistry*, 1999, **38**, 12969–12973.
54 V. Fourmond, C. Greco, K. Sybirna, C. Baffert, P.-H. Wang, P. Ezanno, M. Montefiori, M. Bruschi, I. Meynial-Salles, P. Soucaille, J. Blumberger, H. Bottin, L. De Gioia and C. Léger, *Nat. Chem.*, 2014, **6**, 336–342.
55 M. Senger, K. Laun, F. Wittkamp, J. Duan, M. Haumann, T. Happe, M. Winkler, U.-P. Apfel and S. T. Stripp, *Angew. Chem., Int. Ed.*, 2017, **56**, 16503–16506.
56 S. Mebs, M. Senger, J. Duan, F. Wittkamp, U.-P. Apfel, T. Happe, M. Winkler, S. T. Stripp and M. Haumann, *J. Am. Chem. Soc.*, 2017, **139**, 12157–12160.
57 P. Chernev, C. Lambertz, A. Brünje, N. Leidel, K. G. V. Sigfridsson, R. Kositzki, C.-H. Hsieh, S. Yao, R. Schiwon, M. Driess, C. Limberg, T. Happe and M. Haumann, *Inorg. Chem.*, 2014, **53**, 12164–12177.
58 W. Roseboom, A. L. De Lacey, V. M. Fernandez, E. C. Hatchikian and S. P. J. Albracht, *JBIC, J. Biol. Inorg. Chem.*, 2006, **11**, 102–118.
59 H. J. Reich and R. J. Hondal, *ACS Chem. Biol.*, 2016, **11**, 821–841.
60 H. Abul-Futouh, M. El-khateeb, H. Görls, K. J. Asali and W. Weigand, *Dalton Trans.*, 2017, **46**, 2937–2947.
61 M. Birringer, S. Pilawa and L. Flohé, *Nat. Prod. Rep.*, 2002, **19**, 693–718.
62 D. W. Mulder, E. S. Boyd, R. Sarma, R. K. Lange, J. A. Endrizzi, J. B. Broderick and J. W. Peters, *Nature*, 2010, **465**, 248–251.
63 A. Silakov, C. Kamp, E. Reijerse, T. Happe and W. Lubitz, *Biochemistry*, 2009, **48**, 7780–7786.
64 C. V. Popescu and E. Münck, *J. Am. Chem. Soc.*, 1999, **121**, 7877–7884.
65 A. S. Pereira, P. Tavares, I. Moura, J. J. G. Moura and B. H. Huynh, *J. Am. Chem. Soc.*, 2001, **123**, 2771–2782.
66 A. Adamska, A. Silakov, C. Lambertz, O. Rüdiger, T. Happe, E. Reijerse and W. Lubitz, *Angew. Chem., Int. Ed.*, 2012, **51**, 11458–11462.
67 R. H. Crabtree, *Chem. Rev.*, 2016, **116**, 8750–8769.
68 D. W. Mulder, Y. Guo, M. W. Ratzloff and P. W. King, *J. Am. Chem. Soc.*, 2017, **139**, 83–86.
69 D. W. Mulder, M. W. Ratzloff, M. Bruschi, C. Greco, E. Koonce, J. W. Peters and P. W. King, *J. Am. Chem. Soc.*, 2014, **136**, 15394–15402.
70 V. Pelmenschikov, J. A. Birrell, C. C. Pham, N. Mishra, H. Wang, C. Sommer, E. Reijerse, C. P. Richers, K. Tamasaku, Y. Yoda, T. B. Rauchfuss, W. Lubitz and S. P. Cramer, *J. Am. Chem. Soc.*, 2017, **139**, 16894–16902.
71 G. Filippi, F. Arrigoni, L. Bertini, L. De Gioia and G. Zampella, *Inorg. Chem.*, 2015, **54**, 9529–9542.
72 M. E. Carroll, B. E. Barton, T. B. Rauchfuss and P. J. Carroll, *J. Am. Chem. Soc.*, 2012, **134**, 18843–18852.
73 N. Chongdar, J. A. Birrell, K. Pawlak, C. Sommer, E. J. Reijerse, O. Rüdiger, W. Lubitz and H. Ogata, *J. Am. Chem. Soc.*, 2018, **140**, 1057–1068.
74 J. C. Fontecilla-Camps, A. Volbeda, C. Cavazza and Y. Nicolet, *Chem. Rev.*, 2007, **107**, 4273–4303.
75 M. W. W. Adams, *Biochim. Biophys. Acta, Bioenerg.*, 1990, **1020**, 115–145.
76 A. Kubas, C. Orain, D. De Sancho, L. Saujet, M. Sensi, C. Gauquelin, I. Meynial-Salles, P. Soucaille, H. Bottin, C. Baffert, V. Fourmond, R. B. Best, J. Blumberger and C. Leger, *Nat. Chem.*, 2017, **9**, 88–95.
77 K. D. Swanson, M. W. Ratzloff, D. W. Mulder, J. H. Artz, S. Ghose, A. Hoffman, S. White, O. A. Zadvornyy, J. B. Broderick, B. Bothner, P. W. King and J. W. Peters, *J. Am. Chem. Soc.*, 2015, **137**, 1809–1816.
78 M. Winkler, S. Kuhlgert, M. Hippler and T. Happe, *J. Biol. Chem.*, 2009, **284**, 36620–36627.
79 J. H. Artz, D. W. Mulder, M. W. Ratzloff, C. E. Lubner, O. A. Zadvornyy, A. X. LeVan, S. G. Williams, M. W. W. Adams, A. K. Jones, P. W. King and J. W. Peters, *J. Am. Chem. Soc.*, 2017, **139**, 9544–9550.
80 D. Adam, L. Bösche, L. Castañeda-Losada, M. Winkler, U.-P. Apfel and T. Happe, *ChemSusChem*, 2017, **10**, 894–902.
81 P. Rodríguez-Maciá, K. Pawlak, O. Rüdiger, E. J. Reijerse, W. Lubitz and J. A. Birrell, *J. Am. Chem. Soc.*, 2017, **139**, 15122–15134.
82 M. Winkler, J. Esselborn and T. Happe, *Biochim. Biophys. Acta, Bioenerg., 2013*, 1827, 974–985.
83 M. Mirmohades, A. Adamska-Venkatesh, C. Sommer, E. Reijerse, R. Lomoth, W. Lubitz and L. Hammarström, *J. Phys. Chem. Lett.*, 2016, **7**, 3290–3293.
84 B. L. Greene, G. E. Vansuch, B. C. Chica, M. W. W. Adams and R. B. Dyer, *Acc. Chem. Res.*, 2017, **50**, 2718–2726.
85 B.-J. Schultz, H. Mohrmann, V. A. Lorenz-Fonfria and J. Heberle, *Spectrochim. Acta, Part A*, 2018, **188**, 666–674.
86 S. K. Gaßmeyer, J. Wetzig, C. Mügge, M. Assmann, J. Enoki, L. Hilterhaus, R. Zuhse, K. Miyamoto, A. Liese and R. Kourist, *ChemCatChem*, 2016, **8**, 916–921.